2023-05-17

Performance evaluation of in situ Fenton-mediated photocatalysis of industrial dye effluent with enhanced TiO2 nanoparticle

Oyetade, Joshua

IWA Publishing

https://doi.org/10.2166/aqua.2023.027

corrected Proof

AQUA
Water Infrastructure, Ecosystems and Society

IWA PUBLISHING

AQUA — Water Infrastructure, Ecosystems and Society Vol 00 No 0, 1 doi: 10.2166/aqua.2023.027

Performance evaluation of *in situ* Fenton-mediated photocatalysis of industrial dye effluent with enhanced TiO_2 nanoparticle

Joshua Akinropo Oyetade *, Askwar Hilonga and Revocatus Lazaro Machunda

School of Materials, Energy, Water and Environmental Sciences, Nelson Mandela African Institution of Science and Technology, P.O. Box 447, Arusha, Tanzania
*Corresponding author. E-mail: joshuaoyetade@gmail.com; oyetadej@nm-aist.ac

JAO, 0000-0002-0726-8398

ABSTRACT

Effluents resulting from the frequent use of industrial azo dyes in textile operations have posed great toxicological impacts on man and the environment. The limitations of conventional treatment infrastructure necessitate the use of rapid Fenton-mediated catalytic systematic process to tackle the attendant treatment limitations. The study applied *in situ* Fenton-mediation process with constructed low power UV-LED reactor for rapid catalytic treatment of dye-laden effluent using enhanced acid and alkali TiO_2-nanoparticles (Nps) (1–5%, i.e. 1–5 M) at definite experimental conditions, respectively. A comprehensive instrumental study was done to access the morphological, functional and elemental constituents of these nanocatalysts. The performance of the respective catalyst was evaluated using methylene blue (MB) dye at definite experimental conditions of pH, dosage, concentration and irradiation time. The results revealed a mesoporous structural nanocatalyst with increasing surface area after enhanced modification. The optimal experimental conditions of pH and concentration were recorded as 5 and 10 mg/L, respectively; while the most efficient nanocatalyst was 3 wt% alkali-modified TiO_2 (3% Ak-TiO_2) having a degradation efficiency of 89.15% at 90 min of irradiation using 50 mg dosage in contrast to higher irradiation time and catalyst dosage for other catalysts.

Key words: degradation, Fenton-mediation, nanocatalyst, performance, photocatalysis, photon

HIGHLIGHTS

- Development of rapid photocatalytic treatment process with built low-powered UV-LED reactor.
- Use of unique Fenton reagents and *in situ* mediation for effective dye degradation.
- Unique morphological enhancement of nanocatalyst for more effective degradation.

GRAPHICAL ABSTRACT

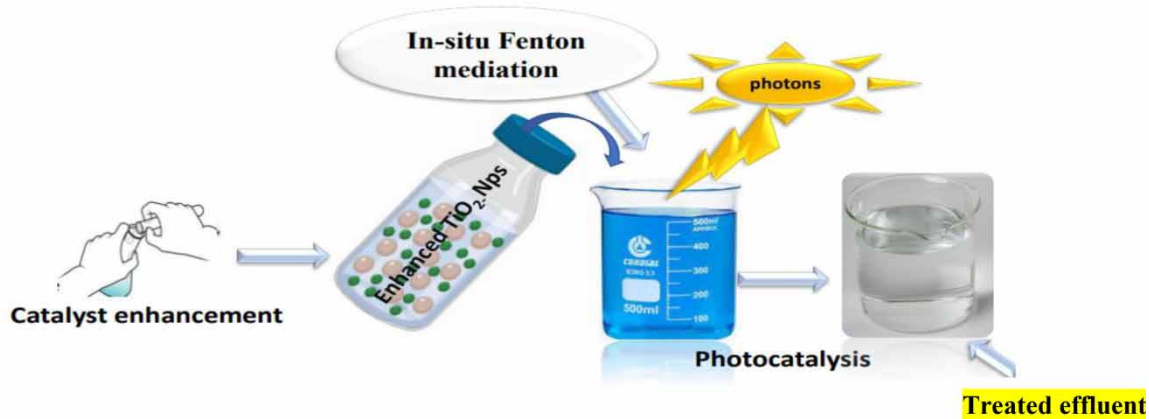

1. INTRODUCTION

The evolution of textile industries and the increasing demands on the use of synthetic dyes corresponds to the generation of a large volume of textile effluent consisting of 10–30% of loosed dyes (Sarmah & Kumar 2011; Al-Rubaie & Mhessn 2012). Among the industrial dyes commonly used are the azo dyes (N = N). This category of dye takes a significant use of 70% among other dyes commercially (Oyetade *et al.* 2022). The industrial attention is based on their vast use in dyeing, printing, pigmentation and extensively in medicine and food colorants (Ameen *et al.* 2011; Kumar & Pandey 2018). Although they are less toxic and chemically stable in raw form, the indiscriminate discharge of their corresponding effluents is deleterious to human health and the environment at large (Kaur & Singhal 2014; Abayomi *et al.* 2020; Deriase *et al.* 2021; Oyetade *et al.* 2023). Treatment technologies categorized as physical, biological and chemical treatments have been applied for the remediation of recalcitrant dye pollutants (Xu *et al.* 2010; Kumar & Pandey 2018). However, the recalcitrant nature and chemo-transformative behavior of the dye molecules in textile wastewater remain challenging (Oyetade *et al.* 2022). In recent times, studies have focused on the use of photocatalysis as an efficient treatment technology to completely mineralize the selected recalcitrant dye pollutants (Xu *et al.* 2010; Zhu *et al.* 2010). Generally, the photocatalytic approach is a photon-induced process occurring which takes place at the surface of photon excited nanocatalysts, such as TiO_2, ZnO h-BN, GO, SnO_2 ZrO_2, ZnO, CdS, Fe_2O_3, and so on (Hou *et al.* 2018). The mechanism involves the capturing of photon energy from light by the photocatalyst, excitation of the electrons from the valence band (VB) to the conduction band (CB) (electron–hole pair), formation of oxidizing and reducing sites, generation of radical species (•OH, $\bullet O^{2-}$ and •OOH) and radical attack which mineralizes the dye molecules (Lopes Colpani *et al.* 2019). The radical attack leads to the degradation of dye molecules into CO_2, H_2O and other harmless substances (Sarmah & Kumar 2011; Hossain *et al.* 2020). Among the wide spectrum of photocatalysts semiconductors used, the selection of titanium dioxide (TiO_2) is based on its cost-effectiveness, nontoxicity, biocompatibility, stability, possibility of recovery and reuse, corrosion resistance, flexibility in synthesis and surface modification with good adsorption–desorption rate (Haider *et al.* 2019). Furthermore, the semiconductor has high surface activity and excellent dye mineralization potential based on its unique oxidizing capacity (Jangid *et al.* 2021). This semiconductor generally exists as anatase, rutile and brookite, although other forms of TiO_2 are hollandite, columbite and ramsdellite which are generally unstable (Haider *et al.* 2019). Among the existing forms, rutile and anatase have the most appreciable use with known synthetic pathways such as the sol–gel method, hydrothermal, microemulsion and micelles, pulse laser deposition, and so on (Mezni *et al.* 2017). The vast applicability of rutile and anatase is based on its high oxidative power, photochemical stability, excellent potential energy of photogenerated electrons and appreciable photocatalytic activity (Macwan *et al.* 2011; Xia *et al.* 2014). However, the challenges of agglomeration of the nanoparticles (Nps), low reaction kinetics, insensitivity to visible light, frequent electron-hole recombination and low sorption properties resulted in the need for simultaneous enhancement of the performance via modification of the surface morphology and application of *in situ* Fenton-mediation for the process (Hou *et al.* 2018; Qutub *et al.* 2022; Oyetade *et al.* 2022; Zhang *et al.* 2021a, 2021b). The incorporation of Fenton-mediation in photocatalysis is based on its ability to generate or increase the availability of more radicals at the catalyst surface via the combination reaction of Fe^{2+} and H_2O_2 under acidic conditions. This action incredibly enhances capturing of photons from UV light and solar light via its association with a modified photocatalyst and the generation of more HO• to initiate an effective dye-radical attack (Li *et al.* 2020; Zhang *et al.* 2021a, 2021b). Hence, this study comparatively investigates the performance of *in situ* mediated photocatalytic degradation of methylene blue (MB) dye with acid- and alkali-enhanced TiO_2-Nps and statistical optimization of the most efficient catalyst for industrial scale-up.

2. MATERIALS

2.1. Chemicals, instruments and glassware

High purity grade (99.5%) titanium dioxide (P25) powder consisting of mixed anatase and rutile phase was purchased at LOBA Chemicals in India. Other reagents such as HCl (37% v/v), H_2SO_4 (97% v/v), anhydrous $FeCl_3$, H_2O_2 (30% $_{V/V}$), NaOH and methylene blue dye MB ($C_{16}H_{18}ClN_3S$) purchased from the same location were analytical grade. Furthermore, de-ionized water was used throughout the experiment, while other glassware and equipment such as a centrifuge machine, analytical weighing balance and oven were procured at the Nelson Mandela African Institution of Science and Technology (NM-AIST), Tanzania. A low power rating (18 W) UV-LED reactor was constructed at Arusha Technical College (ATC) in Tanzania with a power rating of 18 W.

2.2. Preparation of enhanced TiO_2-Nps

Acid enhancement of the nanocatalyst (TiO_2) was carried out according to the modified method reported by Park & Shin (2014) and Hou *et al.* (2018). This involved weighing 1.5 g of TiO_2 into 100 mL of 0,1,2, 3, 4 and 5 mol dm^{-3} concentrations of H_2SO_4 (AC-TiO_2), with stirring for 3 h. The solution was then centrifuged at 3,000 rpm, filtered and washed with ultrapure water three times before drying at 105 °C in the oven for 2 h. The resulting material was calcinated at 450 °C for 2 h to eliminate water trappings in the catalyst matrix and pulverized to obtain powdered material. Each sample was labeled appropriately 0% (untreated TiO_2-Nps) and then 1–5% (i.e. 1–5 M), respectively. The procedure was repeated using NaOH to obtain alkali-modified TiO_2-Nps (AK-TiO_2).

2.3. Nanocatalyst characterization

The morphological properties of prepared samples were analyzed using a Zeiss Ultra Plus 55 Field Emission Scanning Electron Microscope (FE-SEM) at 2.0 KV acceleration potential with energy-dispersive X-ray spectroscopy (EDX). N_2 adsorption–desorption isotherms of the samples were achieved through the aid of a micromeritics TriStar II 3020 device run at a relative pressure (P/P_o) ranging from 0.01 to 1.0 with the samples being pre-degassed at a temperature of 120 °C for 16 h in a vacuum before the analysis was performed. A Brunauer–Emmett–Teller (BET) and Barrett–Joyner–Halenda (BJH) model was adopted to estimate the samples' surface area and pore size distribution (PSD), respectively. X-ray diffraction (XRD) patterns of the samples were recorded on a Bruker D8 Advance X-ray diffractometer with Cu Kα radiation. The Fourier-transform infrared spectra (FT-IR) of the samples were recorded on a Vertex 70 spectrometer in a range from 4,000 to 400 cm^{-1}. The initial and final concentrations of the treated effluent were quantified as a function of the absorbance using UV-Vis diffuse reflectance spectroscopy (UV-vis DRS; Shimadzu 2600, Kyoto, Japan).

2.4. Photocatalytic performance evaluation

Performance evaluation of the photodegradation of the dye molecules (MB) in aqueous solution via the simultaneous use of catalyst with *in situ* Fenton-mediation was studied under constructed cost-effective low-powered UV-LED reactor. Aqueous suspension of MB effluent (100 mL, 10 mg/L) was placed in a 250 mL beaker and a measured amount of the TiO_2-Nps was added. Before irradiation, the suspensions were magnetically stirred in the dark for approximately 60 min. Constant stirring of the suspensions was maintained before and during the irradiation of UV light (Shahabuddin *et al.* 2018). A unique Fenton reagent involving the anhydrous $FeCl_3$ and H_2O_2 was prepared via the modified method of Liu *et al.* (2019) and added *in situ* to the process before irradiation. At a definite time interval, 5 mL of the aliquot was taken and centrifuged at 3,000 rpm. The supernatant was quantified using the UV-Vis at a predetermined λ_{max} of 666 for the MB. Equation (1) was used to determine the degradation efficiency. The same process was carried out for acid (AC-$TiO_{2)}$ and alkali-modified (AK-TiO_2) nanocatalysts at 50, 70, 90 and 110 mg dosages, respectively. The procedure was repeated at the pH range of 3–11, a concentration of 10–40 and an irradiation time of 15–90 min at 50 mg/100 mL of the aqueous solution

$$\%\text{Degradation efficiency} = \frac{C_0 - C_t}{C_0} \times 100 \tag{1}$$

where C_t is the concentration at time t, C_0 initial dye concentration

3. RESULTS AND DISCUSSION

3.1. Morphological characterization of nanocatalysts

The FE-SEM image in Figure 1(a) and 1(b) describes the morphological arrangement of the untreated P25 TiO_2–Nps catalyst, Figure 1(c) and 1(d) depicts the 3% acid and alkali-enhanced catalyst while Figure 1(g) –1(j) shows a 5% enhanced catalyst at different magnifications. From the imaging, a highly stacked and clustered morphological arrangement was observed for untreated TiO_2-NPs in Figure 1(a) and 1(b) and for all the acid-enhanced catalysts. The clustered morphology from the imaging was equally reported by Kumar & Pandey (2018), which is connected with lower binding sites available and undesirable agglomeration. From Figure 1, the structural expression of the catalyst is a spherical cylindrical nanocatalyst with an average diameter of 2.8 mm. These structural features agree with the FE-SEM studied by Sarmah & Kumar (2011) and Zhou *et al.* (2022) on TiO_2-Nps; however, Hou *et al.* (2018) added that the clustered morphological characteristics of the TiO_2-Nps and the acid-enhanced catalyst are often responsible for the agglomeration phenomenon which lowers the photocatalytic

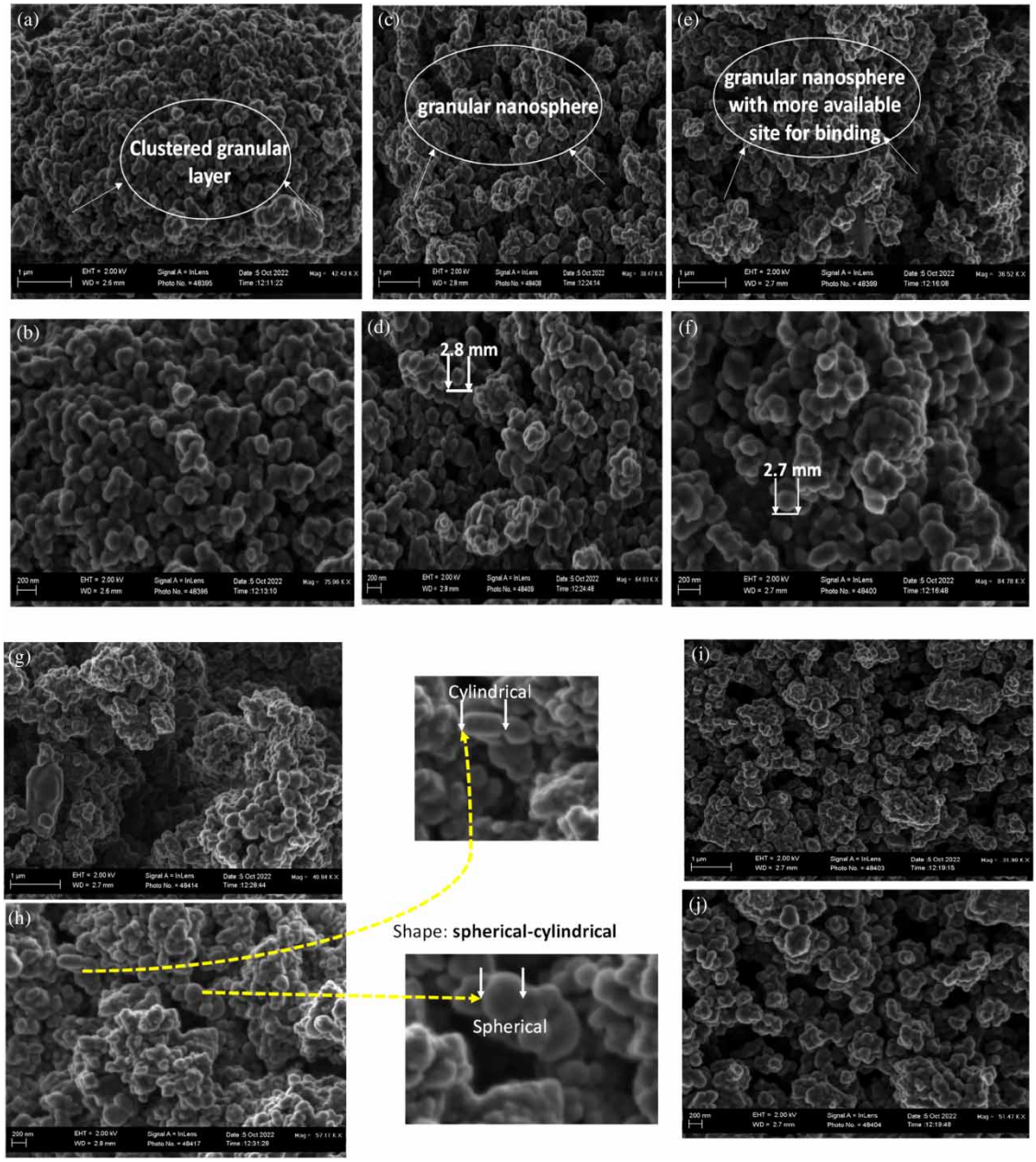

Figure 1 | FE-SEM of (a,b) TiO_2–Nps with 3% AC-TiO_2 (c,d); 3% AK-TiO_2 (e,f); 5% AC-TiO_2 (g,h); 5% AK-TiO_2 (i,j) with their structure.

performance. Also, the cylindrical morphological shape suggests its unique advantage and use as support in the formation of composite via *in situ* polymerization with macromolecules (Zhu *et al.* 2010; Wahyuni *et al.* 2018; Jangid *et al.* 2021). The modification of the surface morphology of synthesized catalysts may facilitate more interparticle spacing and surface growth, thus increasing the availability of active sites for catalyst-adsorbent binding (Zare *et al.* 2018; Lee & Patel 2022; Oyetade *et al.* 2022). The impacts of the treatment, respectively are revealed in terms of the displayed surface growth topology TiO_2-Nps in Figure 2. It is necessary to add that the rutile and the anatase components of TiO_2-Nps are structurally cylindrical as equally exhibited from the imaging in Figure 3 (Hou *et al.* 2018; Haider *et al.* 2019).

3.2. BET analysis

The pattern of the BET adsorption–desorption isotherm in Figure 3(a) and 3(b) structurally describes the features of the pure and enhanced catalyst. The results showcase a typical type IV hysteresis loop of N_2 adsorption–desorption isotherm for all

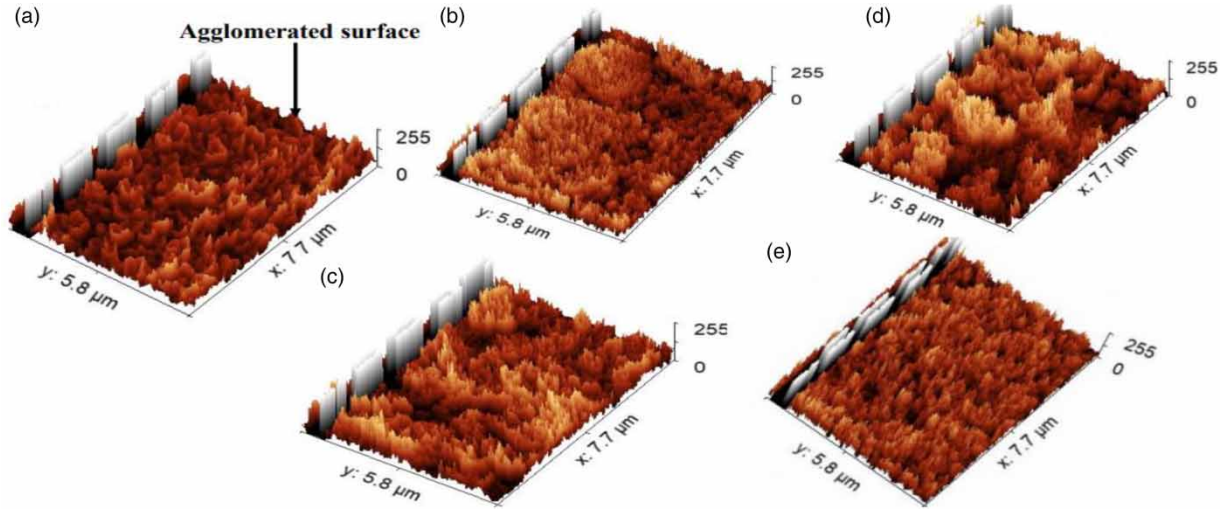

Figure 2 | 3D Surface imaging of TiO_2 (a); (b,c) 3% and (c–e) 5% AC-TiO_2 and AK-TiO_2.

samples, indicating well-developed mesopores (Carja *et al.* 2001; Xiang *et al.* 2010). This report agrees with a similar observation on the mesoporous structure of TiO_2-Nps made by Kumar & Pandey (2018), Liu *et al.* (2019), and Wahyuni *et al.* (2018). From the results, the significant increase in the quantity adsorbed set in at P/P_0 region > 0.8. At this point and beyond, more opening of the hysteresis loop was observed which accounts for stronger multilayer adsorption (Nie *et al.* 2013). Furthermore, the vital features of a specific area, pore diameter and pore volume are described in Table 1, while Figure 3(c) and 3(d) comparatively shows the pore size of 3 and 5% enhanced TiO_2-Nps with its acid and alkali, respectively. From Table 1, the lowest pore size observed was 14.33 nm similar to the 14.73 nm size reported by Hou *et al.* (2018). However, the value increases significantly after respective acid and alkali treatment. This action was similar to the BET surface areas of 47.97 for untreated, while the highest was 91.82 m^2g^{-1} for 3% acid modification followed by 64.74 m^2g^{-1} for 3% alkali modification, respectively. The tunability of the morphological properties increased the surface area of the catalyst, facilitating the prompt electron transport dynamics and high ion diffusion, allowing improved photochemical performance (Carja *et al.* 2001; Mezni *et al.* 2017; Kumar & Pandey 2018).

3.3. XRD analysis

XRD patterns of pure TiO_2-Nps, 3% (Figure 4(a)) and 5% (Figure 4(b)) acid and alkali-enhanced catalysts were, respectively, reported. Figure 4 shows the patterns for pure anatase TiO_2-Nps, at 25°, 38°, 48°, 55.1° and 63.2° which correspond to (101), (103), (200), (211) and (204) planes of TiO_2. However, the structural patterns at the plane (110) correspond to the rutile structure (JCPDS No. 21–1272) (Ananpattarachai *et al.* 2009; Moon *et al.* 2011). The observed features are in agreement with the high purity grade P25 TiO_2 used by Plermjai *et al.* (2019); however, lower than those reported of TiO_2 synthesized via the sol–gel method. From Figure 4(a) and 4(b), it was observed that the intensity of the peaks decreases significantly after the acid and alkali modification process. Furthermore, the higher the intensity of the peaks the more crystalline the arrangement of the Nps, while the decrease in peak intensity suggests the transformation of the surface morphology of the Nps to an amorphous state (Xia *et al.* 2014; Hou *et al.* 2018; López-López *et al.* 2022). This morphological transformation justifies the observed increasing BET surface area and pore volume in Table 1.

3.4. FT-IR analysis

Figure 5 shows the FT-IR spectra of the nanocatalyst with 3% (Figure 8(a)) and 5% (Figure 8(b)) acid- and alkali-enhanced nanocatalyst, respectively. From the spectra, the peak intensity around 400–800 cm^{-1} reveals the functional characteristic of the metal oxide bond (Ti–O bond), while the peak at 1,400 cm^{-1} shows stretching vibrations of Ti–O–Ti (Wang *et al.* 2015; Hou *et al.* 2017). The functional features at this region may facilitate the dye-adsorbent coordination in adsorption which enhances the improved photocatalytic performance of the nanomaterial (Abebe *et al.* 2020). Also in Figure 5, the bend of O–H observed at 3,454.51 cm^{-1} is often assigned to the OH free radical associated with hydrogen bond

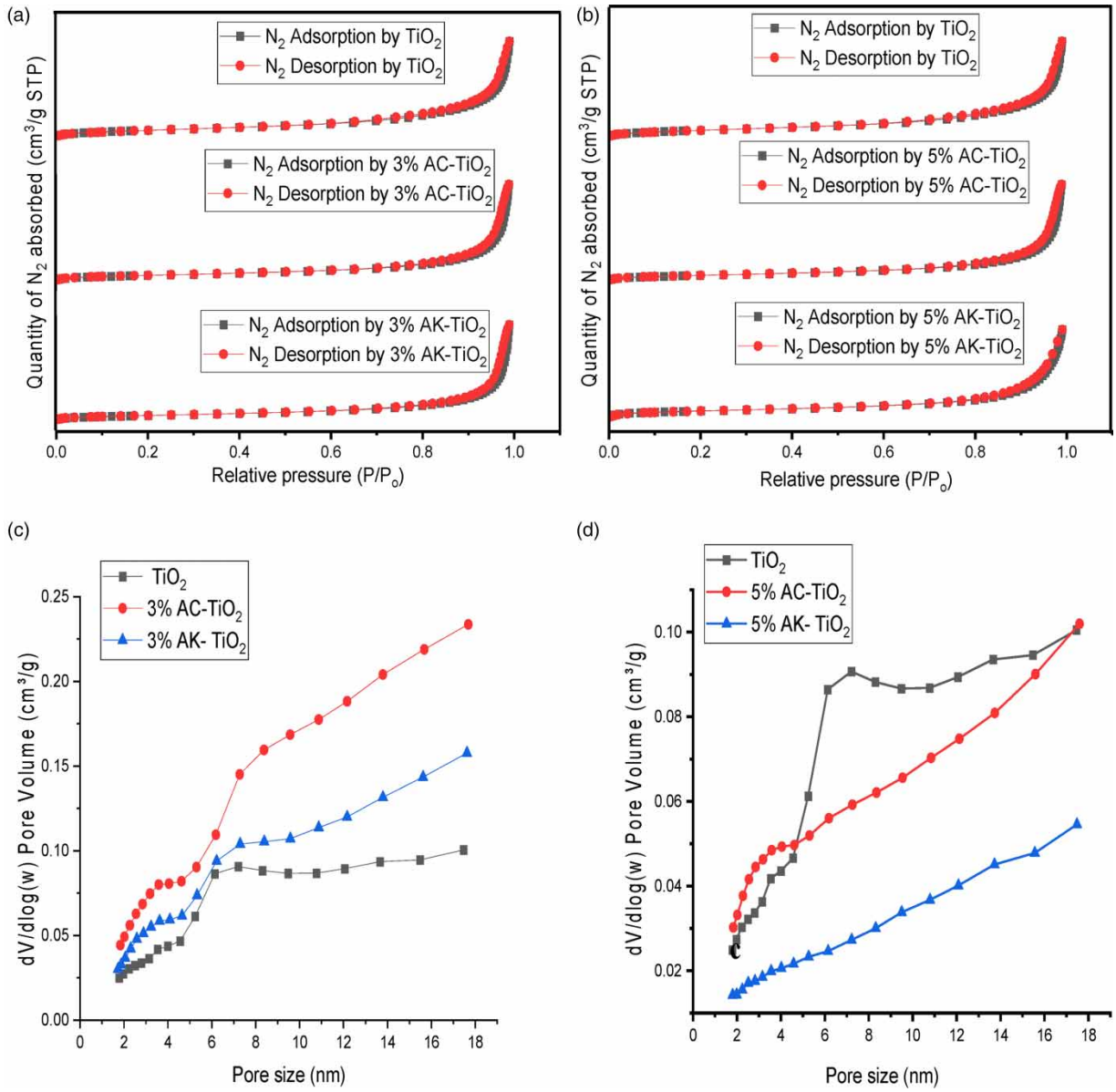

Figure 3 | BET adsorption–desorption isotherm of 3% (a) and 5% (b) and pore size distribution of TiO_2-Nps with enhanced nanocatalyst of 3% (e) and 5% (e) of TiO_2-Nps with enhanced nanocatalyst.

Table 1 | Physicochemical properties of the samples

S/N	Samples	BET surface area ($m^2\ g^{-1}$)	Pore volume (cm^3/g)	Pore size (nm)
1	TiO_2	47.9654	0.17	14.22
2	3% AC-T	91.8267	0.42	18.33
3	5% AC-T	60.5754	0.32	21.28
4	3% AK-T	64.7434	0.30	18.37
5	5% AK-T	50.3858	0.21	16.64

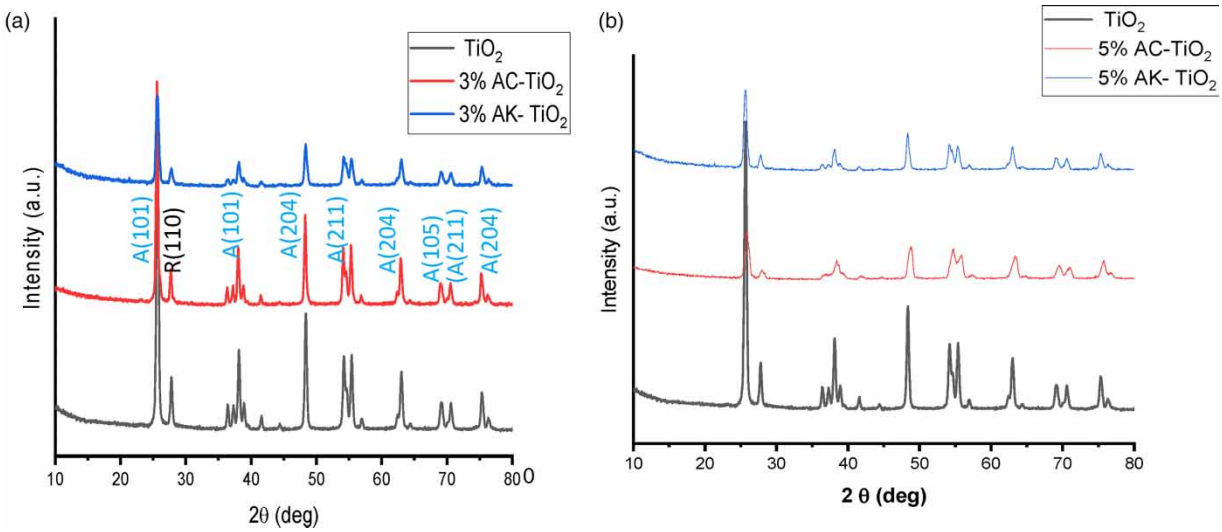

Figure 4 | XRD pattern of TiO_2-Nps with enhanced nanocatalyst of 3% (a) and 5% (b).

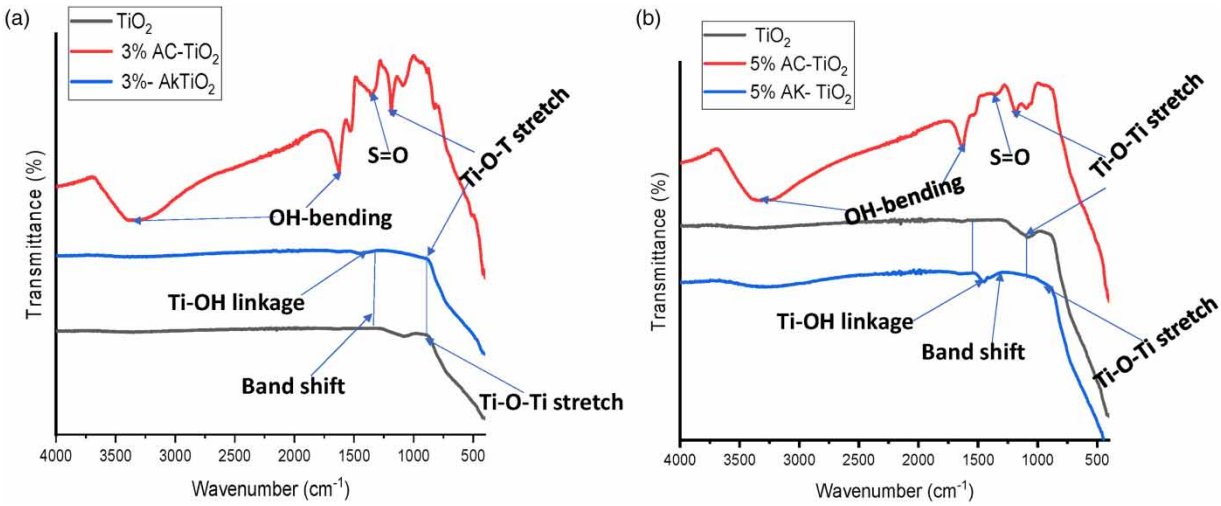

Figure 5 | FT-IR spectra of TiO_2-Nps with enhanced nanocatalyst of 3% (a) and 5% (b).

(Ahmadizadegan 2017; Martakov *et al.* 2018). Additionally, an observed band shift in Figure 5(a) and 5(b) could significantly contribute to the dye coordination and radical formation at the dye-catalyst interphase which improves the catalyst efficiency (Lu & Astruc 2020). The peak at 1,417 cm^{-1} corresponds to the S = O linkage on the acid-enhanced catalyst with increasing intensity at 5%. This band shows the presence of sulfate ions which may act as radical scavengers to lower the generation of hydroxyl radicals during photocatalysis (Park & Shin 2014). Generally, the FT-IR spectra band of photocatalyst interprets the functionality of the material and the bond existing within the atoms, and these forecast the expected reaction mechanism and rate of reaction (Shahabuddin *et al.* 2018; Abebe *et al.* 2020; Oyetade *et al.* 2022).

3.5. EDX analysis

The elemental composition and the percentage abundance are described in Table 2. Table 2 reveals that the predominant elemental composition of Ti (29.91%), O_2 (47.74%) and Si (22.35%) were present in the pure TiO_2-Nps which agrees with the observed functional features of the FT-IR spectra band in Figure 5. However, with alkaline modification the percentage abundance of Ti increases to 54.46 and 59.63% in 3 and 5% acid modification, respectively. On the other hand, the highest

Table 2 | EDX elemental composition

S/N	Samples	Percentage elemental composition (%)						
		Ti	O	Na	Si	Cl	S	Al
1	TiO_2	29.91	47.74	–	22.35	–	–	–
2	3% AC-T	54.46	43.24	–	1.86	–	0.44	–
3	5% AC-T	59.63	37.69	–	2.22	–	0.47	–
4	3% AK-T	58.96	38.98	0.77	0.44	0.64	–	0.22
5	5% Ak-T	59.26	39.01	0.79	0.20	0.74	–	–

titanium composition quantified after alkali treatment was 58.96 and 59.26% for 3 and 5% alkali modification, respectively. The sulfur content of 1.86 and 2.22% in 3% AC-TiO_2 and 5% AC-TiO_2 can be attributed to the sulfuric acid treatment while the presence of Na can be attributed to the NaOH treatment of the Nps. It is necessary to add the increase in element composition of titanium to the treatment completely remediate the silicon content of the TiO_2-Nps which could influence the band gap features and the performance of the semiconductor during adsorption and photocatalysis (Martakov *et al.* 2018; Lu & Astruc 2020). Hence, the higher the amount of titanium and oxygen elements present, the more the possibility of effective coordination and bond establishment needed to adsorb dye molecules before photocatalysis (Angkaew & Limsuwan 2012).

3.6. Photocatalytic activities and effects of independent parameters

a. **Performance test of enhanced TiO_2 nanocatalyst**

The results in Figure 6(a) evaluated the preliminary performance of Fenton-mediated TiO_2-Nps enhanced with 1–5 M concentration of H_2SO_4 and NaOH, respectively. The result reveals the minimal performance of 54.6 and 59.14% for acid- and alkali-enhanced nanocatalysts. However, the optimal performance recorded was at 3 M (64.78 and 74.15%) and (60.1 and 74.03%) 5 M, respectively, for acid- and alkali-enhanced nanocatalysts.

A similar performance was recorded by Hou *et al.* (2018), however, at a considerably higher concentration of 10 M NaOH. Furthermore, Park & Shin (2014) added that although the acid treatments of TiO_2 nanoparticle yield hydroxyl and increase the hydrophilicity of the catalyst, the presence of SO_4^{2-} from the H_2SO_4-treated catalyst at some point acts as •OH scavenger which prevents the photocatalytic process. However, it is necessary to add that the *in situ* Fenton-mediation during the process may account for the appreciable dye photodegradation, especially at 3 and 5 M concentrations of acid. The use of Fenton-mediation facilitates the generation of a significant amount of desired ·OH which promotes decolourization of dye molecules adsorbed onto the surface of the modified nanocatalyst (Yasar & Yousaf 2012; Zhang *et al.* 2021a, 2021b).

b. **Effect of pH on photocatalysis**

Figure 6(b) and 6(c) shows the effect of varying pH (3–11) for the Fenton-mediated photocatalytic process using the most efficient acid- and alkali-enhanced catalysts in Figure 6(a). From the results, the optimal pH value of 5 was recorded with degradation efficiency of 51, 59.67, 61.02, 63.67 and 66.02%, respectively, for pure, 3 and 5 M acid- and alkali-enhanced photocatalysts at 45 min. Abdellah *et al.* (2018) suggested that the basic nature of MB and its interaction with and amphoteric catalyst (TiO_2-Nps) accounts for a desired slightly acidic pH (<5.8) which builds up a positively charged surface to establish electrostatic interaction with the dye molecules. Furthermore, the result of the optimal pH of 5 agrees with the study carried out by Jangid *et al.* (2021) and Shahabuddin *et al.* (2018) using MB as a model dye. The higher performance at this pH is because the positive surface of TiO_2-Nps in an acidic medium facilitates the hydroxyl ion generation needed to form radicals (Jiménez *et al.* 2015). Additionally, the $OH^{\cdot}$ concentration increases with the increasing presence of ^{-}OH ions due to the H^{+} ions in the acidic medium (Ma *et al.* 2014). Also, the formation of electrostatic interaction between the catalyst and dyes in the effluent and radical generation depend on the pH of the medium (Dresselhaus *et al.* 2018). It is necessary to add that the natural and synthetic dyes are generally called either cationic, anionic or neutral. Thus, the nature of the dye constitutes to its reactivity in effluents and suggests optimal pH for its remediation (Joshi & Shrivastava 2012; Abdellah *et al.* 2018).

c. **Effect of initial concentration on photocatalysis**

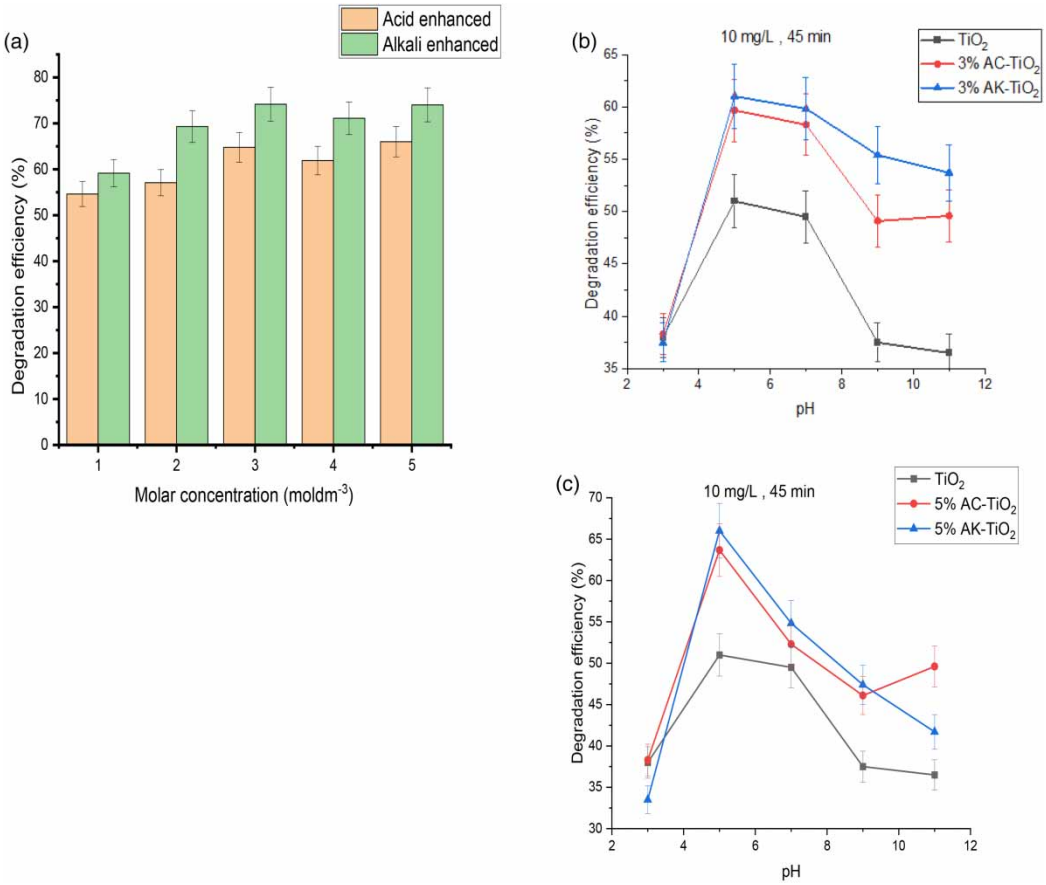

Figure 6 | Preliminary performance test of enhanced TiO_2-Nps at 10 mg/L (a); 1 g/L and 45 min; effect of pH on degradation efficiency of 3% (b) and 5% (c) ehanced TiO_2-Nps.

The effect of initial concentration on the Fenton-mediated process was studied at different concentrations ranging from 10 to 40 mg/L with 50 mg catalyst dosage and 45 min light UV irradiation. Figure 7(a) and 7(b) shows significant reduction with increasing concentration up to 40 mg/L, although we noted optimal concentration of 10 mg/L for the process. Similar optimal concentration was reported by Marziyeh *et al.* (2012), Jangid *et al.* (2021) and Mpelane *et al.* (2020) for MB dye using the

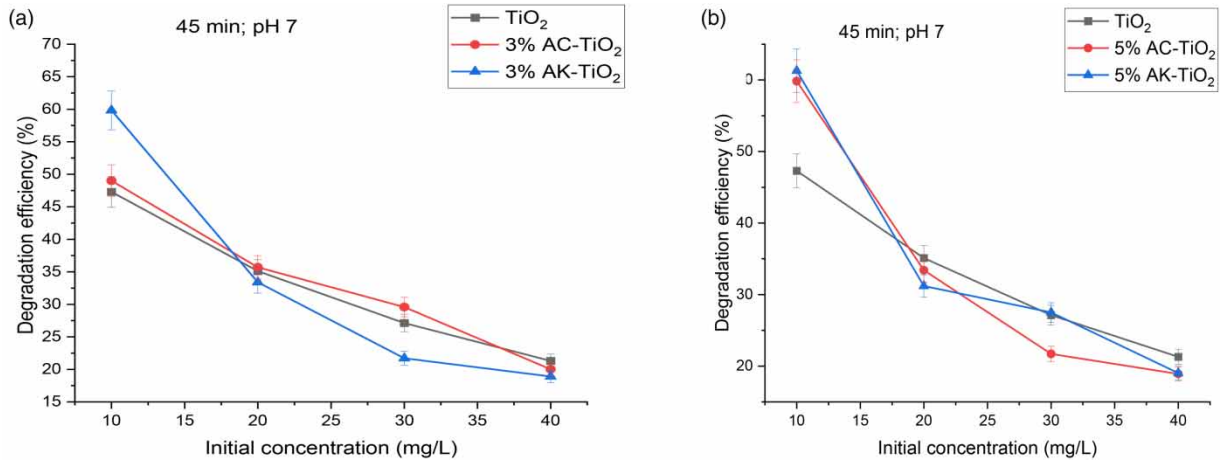

Figure 7 | Effect of initial concentration on degradation efficiency of for 3% (a) and 5% (b) ehanced TiO_2-Nps.

nanocatalyst and with other materials forming composites. The descending plot in Figure 7(a) and 7(b) showcases possible covering and oversaturation of the active sites of the catalyst which reduces dye–photocatalyst interaction. Hence, it lowers the generation of free radicals which enhances dye degradation due to the accessibility of photon energy to the active sites (Marziyeh *et al.* 2012; Dutta *et al.* 2021; Oyetade *et al.* 2022).

d. **Effect of dosage on photocatalysis**

The effect of dosage generally accounts for the reactive performance of the catalyst and its economic implication. Figure 8 reveals the degradation efficiency at different catalyst dosage (30–110 mg) under 45 min UV irradiation, optimum pH (5) and initial concentration of 10 mg/L, respectively. From the results, the optimum dosage ascribed to the pure TiO_2-Nps was 70 mg which slightly increases to 90 mg. However, 50 mg optimal dosage was recorded for 3 and 5 M alkali-enhanced TiO_2-Nps in contrast to 70 mg optimal dosage for acid-enhanced TiO_2-Nps. Beyond this optimal point, there is a level of constancy followed by a gradual decline in performance. From the result, the alkali-enhanced catalyst has an efficiency of 69.3% at 50 mg, compared to 52.65 and 66. 34% degradation at 70 and 90 mg for pure TiO_2-Nps and acid-enhanced TiO_2 (AC-TiO_2-Nps).

The increase in photodegradation is due to the increasing amount of sites available for binding which results in the formation of more active radicals (hydroxyl and superoxide) that initiate the degradation reaction (Suttiponparnit *et al.* 2011; Abdellah *et al.* 2018). Although high catalyst loading of TiO_2 particles impedes incident UV irradiation apart from the possibility of agglomeration owing to clustered surface area (Wang *et al.* 2010; Saleh & Gupta 2012; Abdellah *et al.* 2018). Therefore, beyond the optimal dosage, coupled with a low surface area of the catalyst, reduction in decolorization efficiency is set in, although a similar optimal dosage was recorded by Hou *et al.* (2018) for alkali-enhanced TiO_2 (AK-TiO_2-Nps). On the other hand, Park & Shin (2014) uses 500 mg of acid-enhanced TiO_2 for optimal dye photocatalysis. The significant efficiency of the AK-TiO_2-Nps catalyst is due to the increase in the surface area and lowered agglomeration as revealed by the BET, SEM and 3D surface image, while the saturation and eventual agglomeration with increasing dosages accounts for the gradual reduction of the process (Chatterjee *et al.* 2017; Dutta *et al.* 2021; Bayuo *et al.* 2023). Hence, the surface modification of the nanocatalyst often enhances bonding activities such as electrostatic interactions, Van der Waals forces, hydrogen bonding and π–π interactions which enhance the photocatalytic process, however, at optimal dosage to avoid agglomeration (Ma *et al.* 2014; Jiménez *et al.* 2015).

e. **Effect of irradiation time on photocatalysis**

The degradation efficiency of the Fenton-mediated photocatalysis of MB at varying irradiation times using pure and enhanced TiO_2-Nps as described by Figure 9(a) and 9(b), while Figure 9(c) and 9(d) shows the degradation rate (C_t/C_0) of MB dye over time. From the results, 71.48, 69.01 and 89.15% were recorded for TiO_2, 3% AC-TiO_2 and 3% AK-TiO_2 (3 M), respectively. In contrast, 68.19 and 88.37% for 5% AC-TiO_2, 5% AK-TiO_2 (5 M) were, respectively, quantified.

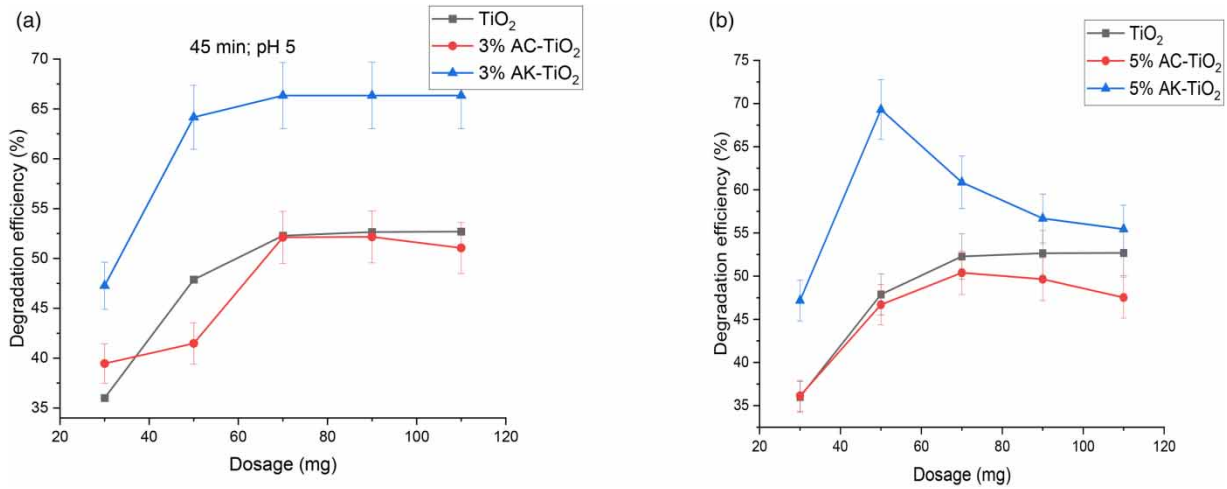

Figure 8 | Effect of catalyst dosage on degradation efficiency for 3% (a) and 5% (b) ehanced TiO_2-Nps.

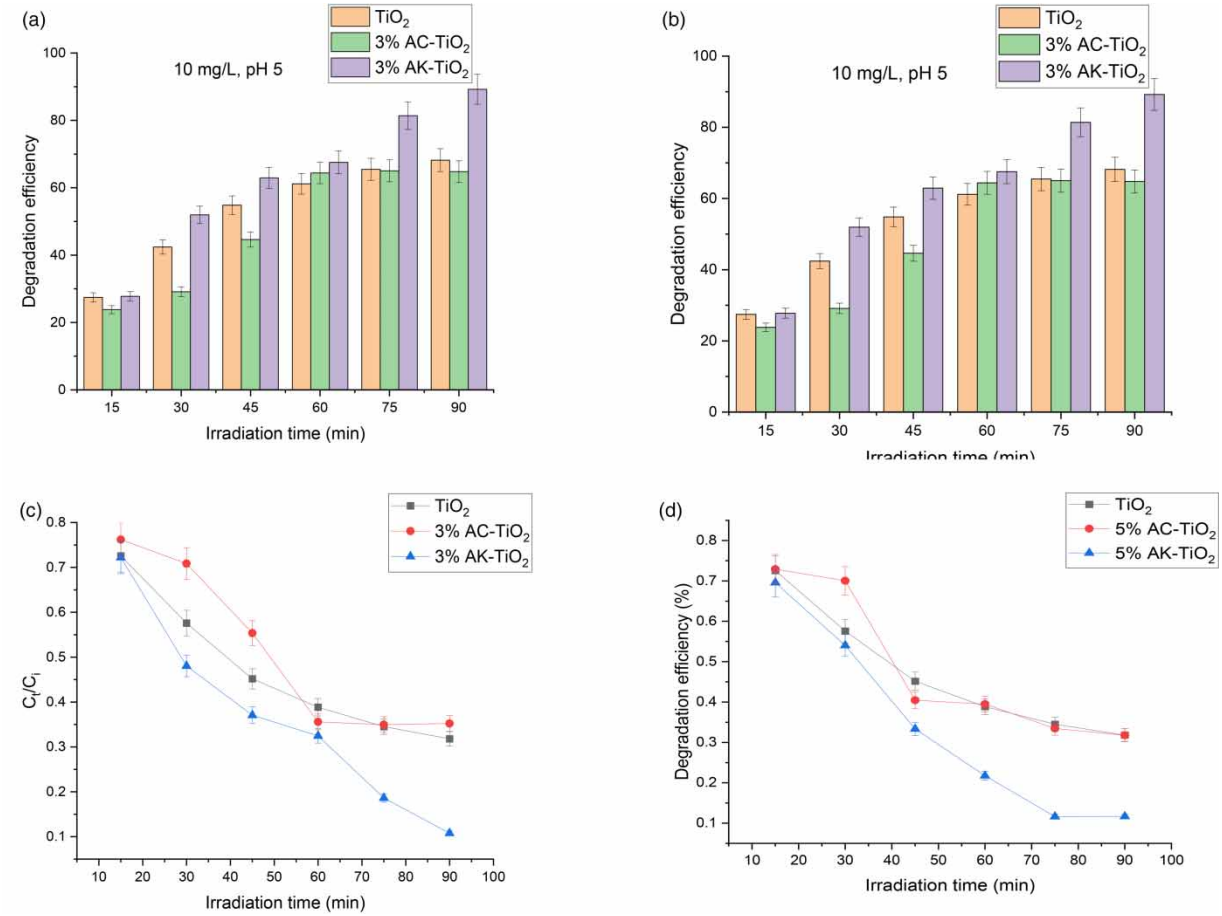

Figure 9 | Effect of irradiation time on (a,b) degradation efficiency and (c,d) degradation rate of MB.

Although a similar amount of degradation was put forward by Hou *et al.* (2018) and Kumar & Pandey (2018) at a higher time range of 120 and 150 min. The lower time rate may be due to the novel application of *in situ* Fenton-mediation to improve the reaction rate of the process using an enhanced catalyst. This accounts for the high radical generation with lower recombination desirable to initiate the radical attack and eventual degradation (Zhang *et al.* 2021a, 2021b). Also, the adoption of *in situ* mediation improves the homogeneity of the solute–solvent interface while facilitating the efficient mass transfer and shorter reaction time (Tunc Dede *et al.* 2019). Although the Fenton-mediation is challenged with the generation of iron sludge, studies revealed that the use of the modified co-photocatalyst (TiO_2-Nps) with the low concentration of iron in the Fenton reagent leads to the generation of little or no iron sludge (Chacó *et al.* 2006; Dong *et al.* 2020). The use of this multiple process is called photo-Fenton where the electron generated by the co-photocatalyst is captured by Fe^{3+} to produce Fe^{2+} which combines again with H_2O_2, thereby preventing covering the surface of the catalyst leading to its deactivation (Mokhbi *et al.* 2019; Dong *et al.* 2020).

Additionally, at an optimum time of 90 min, the lower degradation of acid-enhanced catalyst is due to the possibility of agglomeration as described from the SEM image and inhibition of radical attack as a result of sulfate ion acting as radical scavengers (Abdellah *et al.* 2018; Shahabuddin *et al.* 2018). Furthermore, after the darkroom adsorption–desorption process, at 15 min irradiation, the lower degradation efficiency for all catalysts is due to the generation of fewer electron–hole pairs before radical formation and degradation of adsorbed dye molecules (Jangid *et al.* 2021). However, as time increases, the degradation efficiency increases, respectively. It is worthy of note that the highest efficiency of 89.15 and 88.97% for 3 and 5 M alkali-enhanced TiO_2 indicates the successful modification of the surface morphology as described by the SEM results which enrich the catalyst with significant binding sites and possibly influence its bandgap (Ahmadizadegan 2017; Debnath *et al.* 2021; Oyetade *et al.* 2022). The process of bandgap tunability and surface modification in this regard limits the possibility of agglomeration and recombination of electron–hole pair (Bingham & Daoud 2011; Eskizeybek *et al.* 2012; Jangid *et al.* 2021). Shahabuddin

et al. (2018) added that the larger the surface areas the more active sites available for binding and the lower the agglomeration rate of the nanocomposite. However, the organic dye has light-absorbing potential and can undergo electronic transition via intersystem crossing leading to self-decomposition as the singlets and triplets species are formed (Subramanian *et al.* 2014; Shahabuddin *et al.* 2018). The formation of these species is enhanced by their interaction with photon-active and active site-enriched nanocatalyst which reacts with oxygen and water molecules to generate peroxide, superoxide and hydroxyl radicals. This process is facilitated at a lower time via Fenton-mediation (Shahabuddin *et al.* 2018; Oyetade *et al.* 2022).

3.8. Reaction mechanism

The surface modification via alkali modification is significant in charge separation during the photocatalytic process. The preliminary adsorption–desorption in a dark room establishes an electrostatic bond and enhances the adsorbent–adsorbate linkage between TiO_2-Nps and MB dye (Figure 10). Irradiation of the system with UV-LED results in the excitation of electrons from the valance band to the CB with appreciable charge separation due to the preliminary alkali modification process.

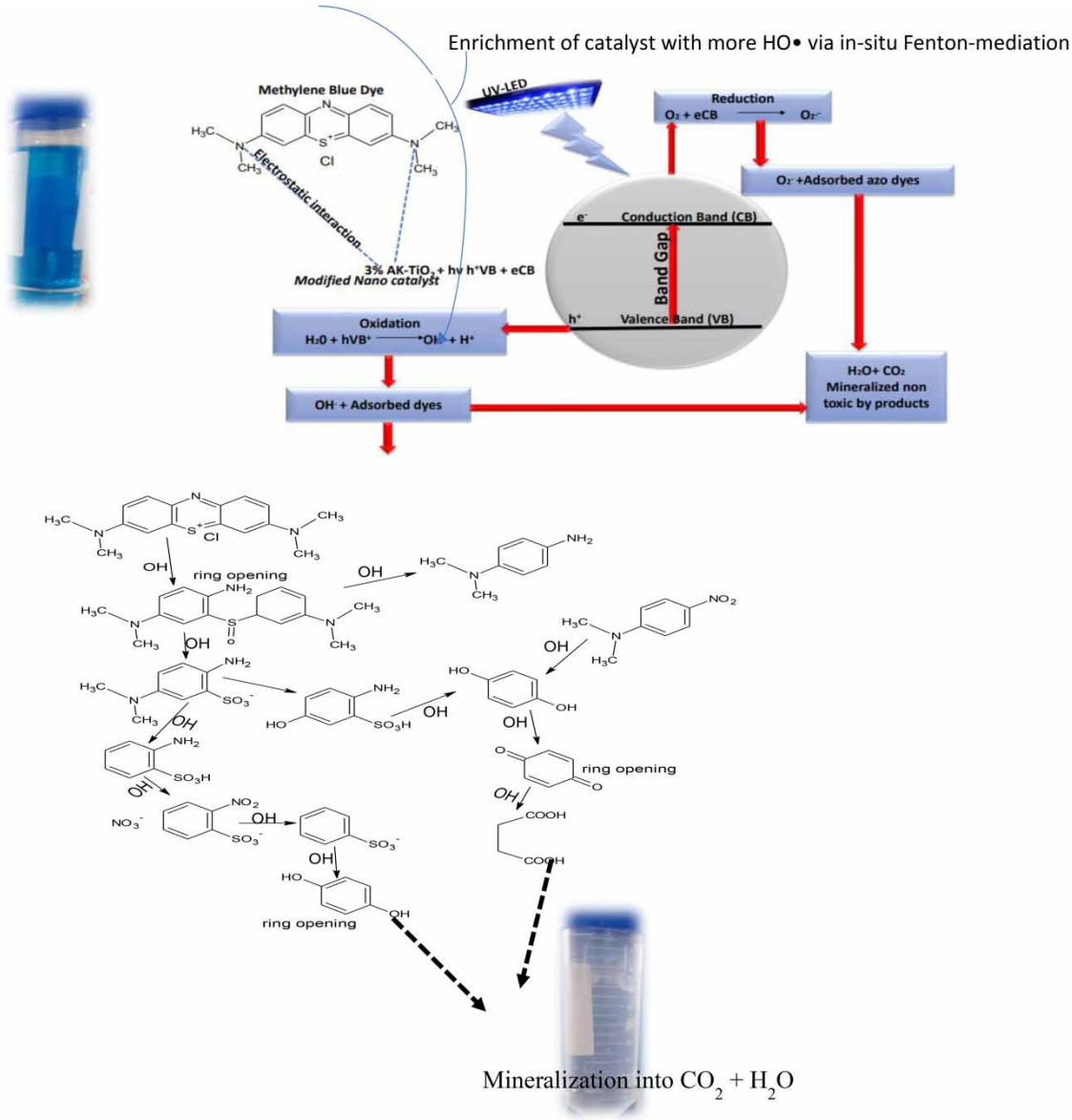

Figure 10 | Reaction mechanism.

Radicals such as hydroxyl radicals (OH•), superoxide radical anions ($O\bullet^{2-}$) and hydroperoxyl radicals (•OOH) are generated during this process (Zangeneh *et al.* 2015; Qamar *et al.* 2019). Also at the optimal pH of 5 (slightly acidic condition), the surface of the amphoteric photocatalyst (TiO_2-Nps) becomes positively charged, thereby establishing electrostatic reaction with the negatively charged model dye (MB), this process facilitates effective adsorption of the dye molecules unto the surface of the catalyst before the radical attack on irradiation (Jiménez *et al.* 2015; Abdellah *et al.* 2018). During the irradiation process, a spontaneous and simultaneous redox reaction alongside a radical attack of the adsorbed dye molecules occurs, leading to the preliminary opening of the ring as described in Figure 10. However, the *in situ* mediation of the process by Fenton reagents accounts for the generation of a larger amount of radical which combines with the radical generated by the action of the nanocatalyst in Equations (3)–(7). The reaction eventually terminates at the point of mineralization of the dye molecules into CO_2 and H_2O which is reflected in decolorization of the effluent in Figure 10 (Asghar *et al.* 2015; Jangid *et al.* 2021).

$$H_2O_2 + hv \rightarrow 2HO\bullet \tag{3}$$

$$3FeCl_3 + H_2O \rightarrow Fe_2O_3 + HCl \tag{4}$$

$$Fe_2O_3 + hv \rightarrow Fe^{2+} + HO\bullet \tag{5}$$

$$Fe^{2+} \rightarrow Fe^{3+} \tag{6}$$

$$Fe^{3+} + H_2O_2 + hv \rightarrow Fe^{2+} + HO\bullet + H^+ \tag{7}$$

3.9. Comparison of degradation efficiency

The performance of the most effective enhanced TiO_2 (3% AK-TiO_2) is compared with other reports at optimal experimental conditions for the degradation of MB in Table 3. From the comparative results, the use of *in situ* Fenton-mediated photocatalysis and enhanced catalyst (3% AK-TiO_2) shows appreciable efficiency in contrast to reagents such as rihodizonic acid and salicylic acid used apart from their reported toxicity and cost intensiveness. Furthermore, a lower amount of NaOH

Table 3 | Comparison between the present study and reported TiO_2-enhanced catalyst for photodegradation of MB dye

Nanocatalyst	pH	Initial conc (mg/L)	Source	Catalyst dosage (mg)	Irradiation time (min)	Efficiency (%)	References
10 M NaOH-treated TiO_2	–	10	300 W Xenon lamp	20	150	–	Hou *et al.* (2018)
Fenton-mediated-3% AK-TiO_2-Nps	5	10	18 W UV-LED	50	90	89.15	Present study
TiO_2 (rod)	7	10	100 W Xenon lamp	50	90	25.03	Wahyuni *et al.* (2018)
TiO_2-NPs	7	10	30 W UVC lamp	100	150	28	Koysuren & Koysuren (2019)
TiO_2 Nanopowder	11	10	24 W Hitachi black light lamp	30	60	85	Marziyeh *et al.* (2012)
Commercial TiO_2 particles.	3	10^{-5}	UV lamp	70	60	99	Yuangpho *et al.* (2018)
H_2O_2/TiO_2	2	20	39 W/m^2 UV lamp with light intensity	150	80	97.6	Farouq (2018)
TiO_2-Nps	–	10	Visible	100	150	50	Melinte *et al.* (2019)
TiO_2_SF	–	10	300 W Xenon lamp	200	120	54	Xu *et al.* (2020)
Ti-SA	6	2×10^{-6}	400 W UV light	200	180	93.3	Mohammadi & Aliakbarzadeh Karimi (2017)
NF/TiO_2_RA		10	150 W high-pressure xenon	10	90	60	Sun *et al.* (2020)

RA, rhodizonic acid; SS, salyscilic acid; Nf, nano fiber; Nr, nano rods; Nps, nanoparticles.

concentration is required for the current study compared to the 10 M NaOH used by Hou *et al.* (2018). However, it is necessary to add that the variation in the light sources from Table 3 greatly influences the efficiency. Hence, at a shorter time and with cost-effective energy, the economically viable nanocatalyst can be applicable for optimal remediation of effluent laden with recalcitrant dyes thereby addressing environmental concerns and contributing to the sustainable development goal (6) clean water and sanitation, goal (7), affordable energy (14) life below water and goal (15) life on land. Furthermore, the modification creates the possibility of recycling and reuse of the photocatalyst without additional treatment due to lowered agglomeration from the alkali enhancement and the conversion of Fe^{3+} to Fe^{2+} via the capturing of the electron generated from the redox process of the catalyst (AK-TiO_2-Nps) (Dong *et al.* 2020; Bilici *et al.* 2021). Also, when coupled without other photon-sensitive nanomaterials or immobilized on nanopolymeric support leaching is reduced and a higher recovery yield for reuse is obtainable (Oyetade *et al.* 2022)

4. CONCLUSION

In summary, the Fenton-mediated photocatalytic process vis-à-vis the enhanced TiO_2-Nps was comprehensively evaluated and statistically modeled by the optimization of the independent variable factors for degradation of industrially used azo dye (MB). The XRD result reveals the predominate peak of anatase with rutile, while the SEM imaging indicated modified surface morphology having a mesoporous structure from the BET isotherm. The availability of more pore size and active sites after alkali modification is in tandem with the higher degradation efficiency coupled with the *in situ* mediation of the process by the Fenton reagent to generate more radicals. Furthermore, the study reveals that the slightly acidic pH of the medium enhanced the presence of H^+ ions which increase ^-OH necessary for the generation of the desired hydroxyl radicals. Hence, at a slightly acidic medium, alkali-modified TiO_2-Nps performs most effectively in the mineralization of organic dye pollutants.

4.1. Recommendations

1. The use of Fenton-mediated process at measured effluent concentration influences the efficiency of the process.
2. Development of nanocatalyst trapping system to recover and reuse catalyst for effluent decolorization.
3. Reuse of treated water for basic industrial operations such as desizing, singeing, and cooling of boilers.
4. Development of CO_2 sequestration system to capture the gas resulting in photocatalysis in further industrial process.

ACKNOWLEDGEMENTS

This work was supported and funded by the Regional Scholarship for Innovation Fund (RSIF), a flagship program of the Partnership for Skills in Applied Sciences, Engineering and Technology (PASET).

DATA AVAILABILITY STATEMENT

All relevant data are included in the paper or its Supplementary Information.

CONFLICT OF INTEREST

The authors declare there is no conflict.

REFERENCES

Abayomi, A., Jamiu, J., Joshua, O., Judith, U., Taiwo, A. & Moyo, F. 2020 Preparation and performance evaluation of an active anti-bleeding solution for laundering multicoloured textile apparels. *Chemistry Journal* **5** (1), 1–14.

Abdellah, M. H., Nosier, S. A., El-Shazly, A. H. & Mubarak, A. A. 2018 Photocatalytic decolorization of methylene blue using TiO_2/UV system enhanced by air sparging. *Alexandria Engineering Journal* **57** (4), 3727–3735. https://doi.org/10.1016/j.aej.2018.07.018.

Abebe, B., Ananda Murthy, H. C. & Dessie, Y. 2020 Synthesis and characterization of Ti–Fe oxide nanomaterials: adsorption–degradation of methyl orange dye. *Arabian Journal for Science and Engineering* **45** (6), 4609–4620.

Ahmadizadegan, H. 2017 Surface modification of TiO_2 nanoparticles with biodegradable nanocellolose and synthesis of novel polyimide/cellulose/TiO_2 membrane. *Journal of Colloid and Interface Science* **491**, 390.

Al-Rubaie, L. A. A. R. & Mhessn, R. J. 2012 Synthesis and characterization of Azo dye para red and new derivatives. *E-Journal of Chemistry* **9** (1), 465–470. https://doi.org/10.1155/2012/206076.

Ameen, S., Akhtar, M. S., Kim, Y. S., Yang, O. & Shin, H.-S. 2011 Polyaniline/gallium doped ZnO heterostructure device via plasma enhanced polymerization technique: preparation, characterization and electrical properties. *Microchimica Acta* **172** (3), 471–478.

Ananpattarachai, J., Kajitvichyanukul, P. & Seraphin, S. 2009 Visible light absorption ability and photocatalytic oxidation activity of various interstitial N-doped TiO_2 prepared from different nitrogen dopants. *Journal of Hazardous Materials* **168** (1), 253–261.

Angkaew, S. & Limsuwan, P. 2012 Preparation of silver-titanium dioxide core-shell (Ag@ TiO_2) nanoparticles: effect of Ti-Ag mole ratio. *Procedia Engineering* **32**, 649–655.

Asghar, A., Raman, A. A. A. & Daud, W. M. A. W. 2015 Advanced oxidation processes for in-situ production of hydrogen peroxide/hydroxyl radical for textile wastewater treatment: a review. *Journal of Cleaner Production* **87**, 826–838.

Bayuo, J., Rwiza, M. J. & Mtei, K. M. 2023 Non-competitive and competitive detoxification of As (III) ions from single and binary biosorption systems and biosorbent regeneration. *Biomass Conversion and Biorefinery* **1**, 1–28.

Bilici, Z., Bouchareb, R., Sacak, T., Yatmaz, H. C. & Dizge, N. 2021 Recycling of TiO_2-containing waste and utilization by photocatalytic degradation of a reactive dye solution. *Water Science and Technology* **83** (5), 1242–1249.

Bingham, S. & Daoud, W. A. 2011 Recent advances in making nano-sized TiO_2 visible-light active through rare-earth metal doping. *Journal of Materials Chemistry* **21** (7), 2041–2050.

Carja, G., Nakamura, R., Aida, T. & Niiyama, H. 2001 Textural properties of layered double hydroxides: effect of magnesium substitution by copper or iron. *Microporous and Mesoporous Materials* **47** (2–3), 275–284.

Chacó, J. M., Leal, M. T., Sánchez, M. & Bandala, E. R. 2006 Solar photocatalytic degradation of azo-dyes by photo-Fenton process. *Dyes and Pigments* **69** (3), 144–150. https://doi.org/10.1016/j.dyepig.2005.01.020.

Chatterjee, M. J., Ghosh, A., Mondal, A. & Banerjee, D. 2017 Polyaniline-single walled carbon nanotube composite-a photocatalyst to degrade rose bengal and methyl orange dyes under visible-light illumination. *RSC Advances* **7** (58), 36403–36415. https://doi.org/10.1039/c7ra03855k.

Debnath, A., Deb, K., Sarkar, K. & Saha, B. 2021 Low interfacial energy barrier and improved thermoelectric performance in Te-Incorporated polypyrrole. *Journal of Physical Chemistry C* **125** (1), 168–177. https://doi.org/10.1021/acs.jpcc.0c09100.

Deriase, S. F., El-Salamony, R. A., Amdeha, E. & Al-Sabagh, A. M. 2021 Statistical optimization of photocatalytic degradation process of methylene blue dye by SnO–TiO_2–AC composite using response surface methodology. *Environmental Progress & Sustainable Energy* **40** (5), e13639.

Dong, C., Xing, M. & Zhang, J. 2020 Recent progress of photocatalytic fenton-like process for environmental remediation. *Frontiers in Environmental Chemistry* **1**, 1–21. https://doi.org/10.3389/fenvc.2020.00008.

Dresselhaus, M., Dresselhaus, G., Cronin, S. B. & Souza Filho, G. 2018 Absorption of light in solids. In: *Solid State Properties* (M. Dresselhaus, ed.). Springer, Berlin, Heidelberg, pp. 365–389.

Dutta, S., Gupta, B., Srivastava, S. K. & Gupta, A. K. 2021 Recent advances on the removal of dyes from wastewater using various adsorbents: a critical review. *Materials Advances* **2** (14), 4497–4531.

Eskizeybek, V., Sarı, F., Gülce, H., Gülce, A. & Avcı, A. 2012 Preparation of the new polyaniline/ZnO nanocomposite and its photocatalytic activity for degradation of methylene blue and malachite green dyes under UV and natural sun lights irradiations. *Applied Catalysis B: Environmental* **119**, 197–206.

Farouq, R. 2018 Investigation of the kinetics and optimization of photocatalytic degradation of methylene blue. *Journal of the Chinese Chemical Society* **65** (11), 1333–1339. https://doi.org/10.1002/jccs.201800029.

Haider, A. J., Jameel, Z. N. & Al-Hussaini, I. H. M. 2019 Review on: titanium dioxide applications. *Energy Procedia* **157**, 17–29.

Hossain, S. S., Tarek, M., Munusamy, T. D., Rezaul Karim, K. M., Roopan, S. M., Sarkar, S. M., Cheng, C. K. & Rahman Khan, M. M. 2020 Facile synthesis of CuO/CdS heterostructure photocatalyst for the effective degradation of dye under visible light. *Environmental Research* **188**, 109803. https://doi.org/10.1016/j.envres.2020.109803.

Hou, C., Liu, W. & Zhu, J. 2017 Synthesis of NaOH-modified $TiOF_2$ and its enhanced visible light photocatalytic performance on RhB. *Catalysts* **7** (8), 243.

Hou, C., Hu, B. & Zhu, J. 2018 Photocatalytic degradation of methylene blue over TiO_2 pretreated with varying concentrations of NaOH. *Catalysts* **8** (12), 575.

Jangid, N. K., Jadoun, S., Yadav, A., Srivastava, M. & Kaur, N. 2021 Polyaniline-TiO_2-based photocatalysts for dyes degradation. *Polymer Bulletin* **78** (8). https://doi.org/10.1007/s00289-020-03318-w.

Jiménez, M., Ignacio Maldonado, M., Rodríguez, E. M., Hernández-Ramírez, A., Saggioro, E., Carra, I. & Sanchez Perez, J. A. 2015 Supported TiO_2 solar photocatalysis at semi-pilot scale: degradation of pesticides found in citrus processing industry wastewater, reactivity and influence of photogenerated species. *Journal of Chemical Technology & Biotechnology* **90** (1), 149–157.

Joshi, K. M. & Shrivastava, V. S. 2012 Removal of Methylene Blue dye Aqueous Solution Using Photo Catalysis. *International Journal of Nano Dimension* **2012**, 241–252.

Kaur, J. & Singhal, S. 2014 Heterogeneous photocatalytic degradation of rose bengal: effect of operational parameters. *Physica B: Condensed Matter* **450**, 49–53.

Koysuren, O. & Koysuren, H. N. 2019 Photocatalytic activity of polyaniline/Fe-doped TiO_2 composites by in situ polymerization method. *Journal of Macromolecular Science, Part A: Pure and Applied Chemistry* **56** (3), 267–276. https://doi.org/10.1080/10601325.2019.1565548.

Kumar, A. & Pandey, G. 2018 Preparation and photocatalytic activity of TiO_2/PPy/GO for the degradation of rose bengal and Victoria blue dye in visible light in aqueous solution. *Desalination and Water Treatment* **114**, 265–284. https://doi.org/10.5004/dwt.2018.22312.

Lee, J. & Patel, R. 2022 Wastewater Treatment by Polymeric Microspheres : A Review. *Polymers* **14** (9), 1890.

Li, M., Sun, M., Dong, H., Zhang, J., Su, Y. & Qiang, Z. 2020 Enhancement of micropollutant degradation in UV/H_2O_2 process via iron-containing coagulants. *Water Research* **172**, 115497.

Liu, J., Wang, B., Li, Z., Wu, Z., Zhu, K., Zhuang, J., Xi, Q., Hou, Y., Chen, J. & Cong, M. 2019 Photo-Fenton reaction and H_2O_2 enhanced photocatalytic activity of α-Fe_2O_3 nanoparticles obtained by a simple decomposition route. *Journal of Alloys and Compounds* **771**, 398–405.

Lopes Colpani, G., Teresinha Odorcik Dal'Toé, A., Zanetti, M., Carla Frezza Zeferino, R., Luiz Silva, L., Maria Muneron de Mello, J. & Antônio Fiori, M. 2019 Photocatalytic adsorbents nanoparticles. *Advanced Sorption Process Applications*. https://doi.org/10.5772/intechopen.79954.

López-López, J., Tejeda-Ochoa, A., López-Beltrán, A., Herrera-Ramírez, J. & Méndez-Herrera, P. 2022 Sunlight photocatalytic performance of zno nanoparticles synthesized by green chemistry using different botanical extracts and zinc acetate as a precursor. *Molecules* **27** (1). https://doi.org/10.3390/molecules27010006.

Lu, F. & Astruc, D. 2020 Nanocatalysts and other nanomaterials for water remediation from organic pollutants. *Coordination Chemistry Reviews* **408**, 213180.

Ma, J., Yang, M., Sun, Y., Li, C., Li, Q., Gao, F., Yu, F. & Chen, J. 2014 Fabrication of Ag/TiO_2 nanotube array with enhanced photo-catalytic degradation of aqueous organic pollutant. *Physica E: Low-Dimensional Systems and Nanostructures* **58**, 24–29.

Macwan, D. P., Dave, P. N. & Chaturvedi, S. 2011 A review on nano-TiO_2 sol–gel type syntheses and its applications. *Journal of Materials Science* **46** (11), 3669–3686.

Martakov, I. S., Torlopov, M. A., Mikhaylov, V. I., Krivoshapkina, E. F., Silant'ev, V. E. & Krivoshapkin, P. V. 2018 Interaction of cellulose nanocrystals with titanium dioxide and peculiarities of hybrid structures formation. *Journal of Sol-Gel Science and Technology* **88** (1), 13–21.

Marziyeh, S., Hassan, H. & Mohammad, M. 2012 Experimental study of influencing factors and kinetics in catalytic removal of methylene blue with TiO_2 nanopowder. *American Journal of Environmental Engineering* **2** (1), 1–7.

Melinte, V., Stroea, L. & Chibac-Scutaru, A. L. 2019 Polymer nanocomposites for photocatalytic applications. *Catalysts* **9** (12). https://doi.org/10.3390/catal9120986.

Mezni, A., Saber, N. B., Ibrahim, M. M., El-Kemary, M., Aldalbahi, A., Feng, P., Samia Smiri, L. & Altalhi, T. 2017 Facile synthesis of highly thermally stable TiO_2 photocatalysts. *New Journal of Chemistry* **41** (12), 5021–5027. https://doi.org/10.1039/c7nj00747g.

Mohammadi, A. & Aliakbarzadeh Karimi, A. 2017 Methylene blue removal using surface-modified TiO_2 nanoparticles: a comparative study on adsorption and photocatalytic degradation. *Journal of Water and Environmental Nanotechnology* **2** (2), 118–128.

Mokhbi, Y., Korichi, M. & Akchiche, Z. 2019 Combined photocatalytic and Fenton oxidation for oily wastewater treatment. *Applied Water Science* **9** (2), 1–9. https://doi.org/10.1007/s13201-019-0916-x.

Moon, R. J., Martini, A., Nairn, J., Simonsen, J. & Youngblood, J. 2011 Cellulose nanomaterials review: structure, properties and nanocomposites. *Chemical Society Reviews* **40** (7), 3941–3994

Mpelane, A., Katwire, D. M., Mungondori, H. H., Nyamukamba, P. & Taziwa, R. T. 2020 Application of novel c-TiO_2-cfa/pan photocatalytic membranes in the removal of textile dyes in wastewater. *Catalysts* **10** (8), 1–17. https://doi.org/10.3390/catal10080909.

Nie, L., Yu, J., Li, X., Cheng, B., Liu, G. & Jaroniec, M. 2013 Enhanced performance of NaOH-modified Pt/TiO_2 toward room temperature selective oxidation of formaldehyde. *Environmental Science & Technology* **47** (6), 2777–2783.

Oyetade, J. A., Machunda, R. L. & Hilonga, A. 2022 Photocatalytic degradation of azo dyes in textile wastewater by polyaniline composite catalyst – a review. *Scientific African* **17**, e01305.

Oyetade, J. A., Machunda, R. L. & Hilonga, A. 2023 Investigation of functional performance of treatment systems for textile wastewater in selected textile industries in Tanzania. *Water Science and Technology* **87** (3), 584–597.

Park, S.-K. & Shin, H. 2014 Effect of HCl and H_2SO_4 treatment of TiO_2 powder on the photosensitized degradation of aqueous rhodamine B under visible light. *Journal of Nanoscience and Nanotechnology* **14** (10), 8122–8128.

Plermjai, K., Boonyarattanakalin, K., Mekprasart, W., Phoohinkong, K., Pavasupree, S. & Pecharapa, W. 2019 Optical absorption and FTIR study of cellulose/TiO_2 hybrid composites. *Chiang Mai Journal of Science* **46** (3), 618–625.

Qamar, A., Amin, M. R., Grynko, O., Semeniuk, O., Reznik, A. & Moewes, A. 2019 A probe of valence and conduction band electronic structure of lead oxide films for photodetectors. *ChemPhysChem* **20** (24), 3328–3335.

Qutub, N., Singh, P., Sabir, S., Sagadevan, S. & Oh, W.-C. 2022 Enhanced photocatalytic degradation of acid blue dye using CdS/TiO_2 nanocomposite. *Scientific Reports* **12** (1), 1–19. https://doi.org/10.1038/s41598-022-09479-0.

Saleh, T. A. & Gupta, V. K. 2012 Photo-catalyzed degradation of hazardous dye methyl orange by use of a composite catalyst consisting of multi-walled carbon nanotubes and titanium dioxide. *Journal of Colloid and Interface Science* **371** (1), 101–106. https://doi.org/10.1016/j.jcis.2011.12.038.

Sarmah, S. & Kumar, A. 2011 Photocatalytic activity of polyaniline-TiO_2 nanocomposites. *Indian Journal of Physics* **85** (5), 713–726. https://doi.org/10.1007/s12648-011-0071-1.

Shahabuddin, S., Khanam, R., Khalid, M., Sarih, N. M., Ching, J. J., Mohamad, S. & Saidur, R. 2018 Synthesis of 2D boron nitride doped polyaniline hybrid nanocomposites for photocatalytic degradation of carcinogenic dyes from aqueous solution. *Arabian Journal of Chemistry* **11** (6), 1000–1016. https://doi.org/10.1016/j.arabjc.2018.05.004.

Subramanian, E., Subbulakshmi, S. & Murugan, C. 2014 Inter-relationship between nanostructures of conducting polyaniline and the photocatalytic methylene blue dye degradation efficiencies of its hybrid composites with anatase TiO_2. *Materials Research Bulletin* **51**, 128–135.

Sun, Y., Mwandeje, J. B., Wangatia, L. M., Zabihi, F., Nedeljković, J. & Yang, S. 2020 Enhanced photocatalytic performance of surface-modified TiO_2 nanofibers with rhodizonic acid. *Advanced Fiber Materials* **2** (2), 118–122.

Suttiponparnit, K., Jiang, J., Sahu, M., Suvachittanont, S., Charinpanitkul, T. & Biswas, P. 2011 Role of surface area, primary particle size, and crystal phase on titanium dioxide nanoparticle dispersion properties. *Nanoscale Research Letters* **6** (1), 1–8. https://doi.org/10.1007/s11671-010-9772-1.

Tunc Dede, O., Aksu, Z. & Rehorek, A. 2019 Sonochemical degradation of CI reactive orange 107. *Environmental Engineering Science* **36** (2), 158–171.

Wahyuni, S., Kunarti, E. S., Swasono, R. T. & Kartini, I. 2018 Characterization and photocatalytic activity of TiO_2(rod)-SiO_2-polyaniline nanocomposite. *Indonesian Journal of Chemistry* **18** (2), 321–330. https://doi.org/10.22146/ijc.22550.

Wang, F., Min, S., Han, Y. & Feng, L. 2010 Visible-light-induced photocatalytic degradation of methylene blue with polyaniline-sensitized TiO_2 composite photocatalysts. *Superlattices and Microstructures* **48** (2), 170–180. https://doi.org/10.1016/j.spmi.2010.06.009.

Wang, H., Yi, G., Tan, M., Zu, X., Luo, H. & Jiang, X. 2015 Initial reactant controlled synthesis of double layered TiO_2 nanostructures and characterization of its spectra of absorption and photoluminescence. *Materials Letters* **148**, 5–8.

Xia, T., Zhang, W., Wang, Z., Zhang, Y., Song, X., Murowchick, J., Battaglia, V., Liu, G. & Chen, X. 2014 Amorphous carbon-coated TiO_2 nanocrystals for improved lithium-ion battery and photocatalytic performance. *Nano Energy* **6**, 109–118.

Xiang, Q., Lv, K. & Yu, J. 2010 Pivotal role of fluorine in enhanced photocatalytic activity of anatase TiO_2 nanosheets with dominant (0 0 1) facets for the photocatalytic degradation of acetone in air. *Applied Catalysis B: Environmental* **96** (3–4), 557–564.

Xu, S., Zhu, Y., Jiang, L. & Dan, Y. 2010 Visible light induced photocatalytic degradation of methyl orange by polythiophene/TiO_2 composite particles. *Water, Air, & Soil Pollution* **213** (1), 151–159.

Xu, J., Zhang, T. & Zhang, J. 2020 Photocatalytic degradation of methylene blue with spent FCC catalyst loaded with ferric oxide and titanium dioxide. *Scientific Reports* **10** (1), 1–10. https://doi.org/10.1038/s41598-020-69643-2.

Yasar, A. & Yousaf, S. 2012 Solar assisted photo Fenton for cost effective degradation of textile effluents in comparison to AOPs. *Glob. Nest J* **14**, 477–486.

Yuangpho, N., Trinh, D. T. T., Channei, D., Khanitchaidecha, W. & Nakaruk, A. 2018 The influence of experimental conditions on photocatalytic degradation of methylene blue using titanium dioxide particle. *Journal of the Australian Ceramic Society* **54** (3), 557–564.

Zangeneh, H., Zinatizadeh, A. A. L., Habibi, M., Akia, M. & Isa, M. H. 2015 Photocatalytic oxidation of organic dyes and pollutants in wastewater using different modified titanium dioxides: a comparative review. *Journal of Industrial and Engineering Chemistry* **26**, 1–36.

Zare, E. N., Motahari, A. & Sillanpää, M. 2018 Nanoadsorbents based on conducting polymer nanocomposites with main focus on polyaniline and its derivatives for removal of heavy metal ions/dyes: a review. *Environmental Research* **162**, 173–195. https://doi.org/10.1016/j.envres.2017.12.025.

Zhang, Y., Shaad, K., Vollmer, D. & Ma, C. 2021a Treatment of textile wastewater by advanced oxidation processes – a review. *Global Nest Journal* **13** (1), 1–22.

Zhang, Y., Shaad, K., Vollmer, D. & Ma, C. 2021b Treatment of textile wastewater using advanced oxidation processes – a critical review. *Water* **13** (24), 3515.

Zhou, S., Bai, J., Huang, K., Ye, X., Peng, Y. & Lei, M. 2022 Consideration of photoactivity of TiO_2 pigments via the photodegration of methyl orange under UV irradiation. *Materials* **15** (17). https://doi.org/10.3390/ma15176044.

Zhu, Y., Xu, S. & Yi, D. 2010 Photocatalytic degradation of methyl orange using polythiophene/titanium dioxide composites. *Reactive and Functional Polymers* **70** (5), 282–287. https://doi.org/10.1016/j.reactfunctpolym.2010.01.007.

First received 5 February 2023; accepted in revised form 6 May 2023. Available online 17 May 2023